Growth Dynamics Study of the Martensitic Transformation in Fe-30 Pct Ni Alloys: Part I. Quantitative Measurements of Growth Velocity

ZHEN-ZHONG YU and PHILIP C. CLAPP

Previous studies of the growth velocity in athermal martensitic transformations were of an indirect nature in which the size of individual martensite plates could not be determined with precision. The present study focuses on the quantitative analyses of martensitic growth events in an Fe-30 pct Ni alloy in order to determine the growth velocity and the final size of single transformation events directly and simultaneously. Both magnetic induction and acoustic emission (AE) techniques have been employed, and the corresponding analytical methods have been developed. While efforts have been made to minimize possible distortions of transformation signals caused by detectors and signal processing apparatus, it is recognized that the media in which the signals propagate impose a significant distortion on the signals. We have proposed methods to cope with the effect of eddy currents in the magnetic measurements and the frequency-dependent media attenuation in the AE measurements. Two independent experiments in our study have shown a consistent trend of the growth velocity and the final size of martensitic transformation events as a function of temperature. The growth velocity ranges from 0.25 to 0.65 of the shear wave velocity in the material. Several possibilities responsible for the velocity scatter are discussed, and it is suggested that the varying strain conditions under which the martensitic growth events take place play a decisive role in determining the actual growth velocity.

I. INTRODUCTION

CONSIDERABLE effort, both theoretical and experimental, has been expended in the past 40 years on understanding the nucleation, growth, and final morphology of martensitic transformations. Several competing theories[1–4] have been proposed to understand the heterogeneous nature of martensitic nucleation originating from lattice defects. The phenomenological crystallographic theories[5,6,7] have also been developed to predict some aspects of the final morphology of various martensitic transformations. However, little work has been done on either modeling or measuring the growth stage which is among the least understood aspects from a fundamental viewpoint today. Since the growth process is likely to have a substantial effect on the ultimate morphology of the martensite structure, which, in turn, can be expected to have a large impact on its mechanical properties, it is of great importance to bridge the gap in our understanding of the growth dynamics of martensitic transformations.

The key to the growth dynamics of martensitic transformations is the growth velocity of the moving interface and how it is affected by various driving forces and resisting forces in connection with temperature or strain condition in the vicinity of the interface. Nishiyama[8] has classified the rate of martensitic growth into three different velocity regimes. The fastest ("umklapp") is of the order of mechanical twinning velocities and is often associated with athermal martensitic transformations ($v \cong 10^3$ m/s). The intermediate ("schiebung") is of the order of dislocation velocities in slip deformation and is proportional to the degree of undercooling ($v \cong 10^{-3}$ to 10^{-1} m/s). The slowest is associated with thermoelastic growth and is proportional to the cooling rate ($v \cong 5 \times 10^{-4}$ m/s at a cooling rate of 20 °C/s). It is not surprising that more substantial advances have been made in studying the growth dynamics of the slow or intermediate regimes, as compared to the fast velocity one. Reasonably accurate measurements have been made in the former regimes using a hot stage equipped with a movie camera.[9,10,11] Recently, Grujicic, Olson, and Owen[12] made a systematic study, which provides a great deal of insight and information into the growth dynamics of slow-moving martensite, on the interface mobility of slow velocity, thermally activated martensitic transformations. However, the growth dynamics of umklapp martensitic transformations still remain essentially unknown, mainly because of the difficulties involved in the direct and accurate measurement of extremely fast interfacial motion. Previous attempts measured only average ensemble velocities but no single event velocities.

The main goal of the present study has been to measure individual growth velocities of fast-moving (umklapp) interfaces in the athermal martensitic transformation. Recent improvements in acoustic emission and magnetic induction methods are employed to make independent quantitative measurements of growth velocities in an Fe-30 wt pct Ni alloy. As a result of this study, we believe we are able for the first time to measure the major parameters, such as the growth velocity and the final size, for individual martensite plates.

This paper describes the experimental measurements of martensitic growth velocity and the analyses of measured signals. In parallel, a theoretical study of growth

ZHEN-ZHONG YU, formerly Graduate Research Assistant with the Department of Metallurgy, University of Connecticut, is Research Scientist with Advanced Fuel Research, Inc., P.O. Box 18343, East Hartford, CT 06118. PHILIP C. CLAPP, Professor of Metallurgy, is with the Department of Metallurgy and Institute of Materials Science, University of Connecticut, Storrs, CT 06268.

Manuscript submitted August 30, 1988.

dynamics using a molecular dynamics computer simulation, presented in the following paper, was also carried out to investigate the growth velocities as a function of strain conditions and temperature.

II. HISTORY OF GROWTH VELOCITY MEASUREMENTS

Because of the lack of fast wideband recording instruments, early investigations in the 1930's and 40's, using an optical microscope equipped with a movie camera[13] or using a cardiograph,[14] were not able to resolve the extremely short time period of martensitic growth events. The first significant measurement was made by Bunshah and Mehl in 1953 using a resistivity method.[15] They chose an Fe-29.5 pct Ni alloy, because the electrical resistance decreases by about 50 pct upon the transformation from austenite to martensite. Their electronic circuitry and oscilloscope were capable of responding to signals as short as 10^{-8} seconds. They found electrical resistance pulses varying from 0.5×10^{-7} seconds to 5.0×10^{-7} seconds as the grain diameter varied from 0.001 to 0.01 in. Then, they assumed that the length of the martensite plate was approximately the same as the average diameter of the austenite grains for the first generation of martensite plates and that the length of martensite formed at lower temperatures decreased due to the partitioning of the grains by the prior formation of martensite. The way they derived the average growth velocity was to use this roughly estimated length of martensite plates divided by the time of formation measured from the resistivity signals. This very crude estimate of transformation velocity (1000 m/s) corresponded to about one-third the shear velocity of sound and was found to be constant within ±20 pct over the temperature range −20 °C to −195 °C. It is obvious that the accuracy of Bunshah and Mehl's conclusions is questionable, due to the fact that they were not able to relate the measured time of formation to the size of the same transformation event.

Beisswenger and Scheil,[16] followed by Kimmich and Wachtel,[17] extended and improved the same resistivity approach but essentially obtained the same type of averaged results as Bunshah and Mehl. In 1968, Mukherjee,[18] again using resistivity measurements on an Fe-30 at. pct Ni alloy, found the measured time of formation of martensite plates to be in the range of 1×10^{-7} s to 2×10^{-7} s for small signals obtained in a sample with the average grain diameter of 0.02 cm. He noted that this time period was shorter than that obtained in the same range of the grain size by previous resistivity measurements. These small signals were thought to correspond to the formation of single martensites. However, he again assumed that the length of the largest plate was equal to the average grain diameter and found a higher growth velocity, 1.8×10^3 m/s, which corresponded to $0.6\ v_t$, where v_t is the shear wave velocity in the austenite matrix.

Because of the drastic change in magnetization during the martensitic transformation in Fe-Ni alloys, magnetic induction methods may be used to measure the growth rate of fast-moving interfaces, which is very similar to the technique used to measure the Barkhausen effect due to the sudden change in the direction of magnetization of magnetic domains. In 1942, Okamura *et al.*[19] studied the change in magnetization during martensitic transformation in a Ni steel specimen. Because of the slow speed of the oscillograph used, they were only able to record burst signals with a pulse duration of about 10^{-4} s. In 1972, Suzuki and Saito[20] magnetically measured the transformation velocity in an Fe-31 pct Ni alloy using a faster response circuitry. In the brief report on their results, they stated that a single martensite plate formed in 0.5×10^{-7} s and the propagation velocity was 800 m/s, but very little information is given on the details of the measurement. In addition, the recorded magnetic signal in the report shows a typical feature of a multiple "burst" event (a slowly rising voltage ramp carrying a series of ripples), indicating that some type of average velocity was being reported.

Summarizing the previous measurements of growth velocity, one can easily notice a common weakness in all these measurements attempted so far; *i.e.*, none of them was able to make a direct estimate of the growth velocity or, in other words, to relate the time of formation of a particular plate to its corresponding final size. For over three decades, Bunshah and Mehl's work has been recognized as conclusive evidence of the growth velocity in the umklapp martensitic transformation. However, their results showing the growth velocity as being one-third the speed of sound and constant over a wide temperature range are still questionable because of the indirect and qualitative nature of their measurements. To re-examine those conclusions, it is crucial to develop new techniques to bring the velocity measurement up to a direct and quantitative level. Any success in this respect will undoubtedly benefit the study and interpretation of other high-speed moving defects in related areas such as crack propagation in fracture, mechanical twinning, and massive phase transformations, *etc.*

III. IMPORTANT FEATURES OF THE TRANSFORMATION IN Fe-30 PCT Ni ALLOYS

An Fe-30 wt pct Ni alloy was chosen as the specimen in the present study, because the alloy is a typical example of the athermal martensitic transformation and has been used in many previous growth velocity measurements. The equilibrium temperature T_0 (where the free energy difference between austenite and martensite is zero) of this alloy is estimated to be 450 K (177 °C), according to Kaufman and Cohen's thermodynamical calculation.[21] Martensite starts growing at a temperature more than 100 deg below T_0, indicating that a large degree of supercooling is required for the shear-like displacive transformation. The M_s temperature measured by various methods differs, depending on the sensitivity of each measuring technique. Machlin and Cohen[22] found the M_s temperature in an Fe-29.5 pct Ni alloy to be −14 °C by using the resistivity measurement. Hsu, Chen, and Clapp[23] used different techniques to determine M_s in an Fe-29.58 pct Ni alloy. They found M_s = 7.5 °C in the resistivity measurement and M_s = 55 °C in the acoustic emission measurement, which showed much higher sensitivity than that of the resistivity method.

Another distinct feature in an Fe-30 pct Ni alloy is the

"burst phenomenon." A large number of martensite plates may form simultaneously, presumably triggered by a single plate or a few plates formed earlier, which produce a favorable stress wave, or shock wave, to provoke the subsequent avalanche. This autocatalytic process is often accompanied by a marked temperature rise of the specimen (sometimes 20 °C to 30 °C) due to the release of latent heat. The temperature at which the first burst occurs is referred to as the M_b temperature. The M_b temperature is below M_s and is usually affected by the grain size. A finer grain size is often associated with a lower M_b.[22] In an Fe-30 pct Ni alloy used in the present study, it was found that the transformation at M_b was usually accompanied by the largest temperature rise, and the subsequent transformation was temporarily suppressed by the first burst until the temperature of the specimen reached more than 5 °C below M_b. The transformation resumes in the burst fashion until a large fraction of austenite transforms to martensite. The burst-type transformation usually lasts over a temperature range of 20 to 30 deg, which was verified by the signal patterns in our magnetic and acoustic measurements. Hereafter, this temperature range is termed the burst region. It is then reasonable to say that the transformation occurring before and after the burst region appears to be mainly single events, while the transformation within the burst region is associated with multievents in which many plates may overlap within an extremely short time interval.

Some micrographs are presented here to describe the morphology and microstructure of martensite plates in our Fe-30 pct Ni alloy. Figure 1 represents the as-quenched microstructure of the alloy at room temperature. It contains virtually untransformed austenite grains, except for a very few martensite plates (in the right-hand side) which appear not to traverse the entire austenite grain. Figure 2 shows a micrograph right after the first burst (−15 °C) in which fully grown martensite plates either "partition" the austenite grains or are stopped by pre-existing plates or lattice defects. The morphology of martensite plates exhibits a platelike or lenticular shape with a straight central plane known as the "midrib" and an irregular interface between the martensite and austenite. The midrib plane is widely accepted to be the "habit plane" of the martensitic transformation.

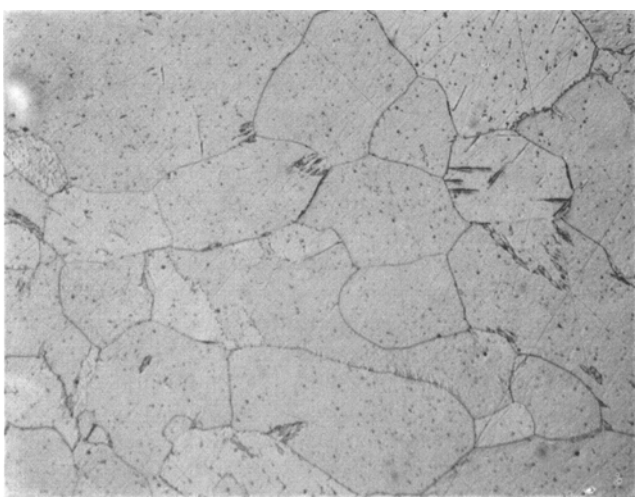

Untransformed Sample, x100 (room temp.)

Fig. 1 — As-quenched microstructure of Fe-30 wt pct Ni alloy. The microstructure at room temperature shows nearly 100 pct austenite grains with a few martensite plates that appear not to traverse the entire grain. Magnification 73 times.

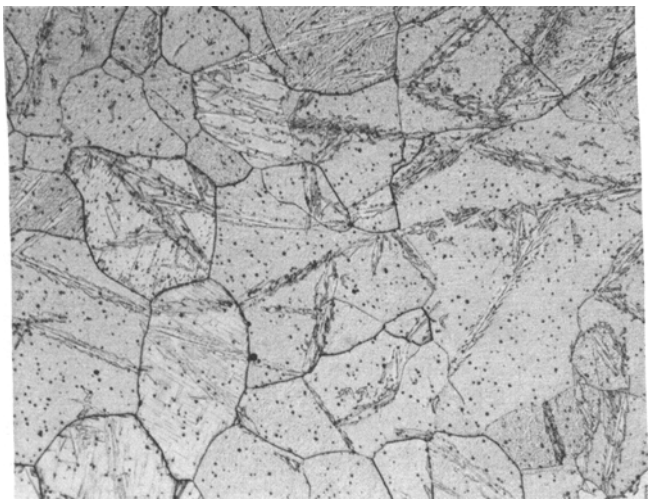

Microstructure Right After the Burst

x100 (−15 °C)

Fig. 2 — Microstructure right after the first burst. The microstructure at −15 °C shows the autocatalytic formation of many martensite plates. Most plates traverse the entire grain, and some plates are in contact at grain boundaries with differently oriented growth directions. Magnification 73 times.

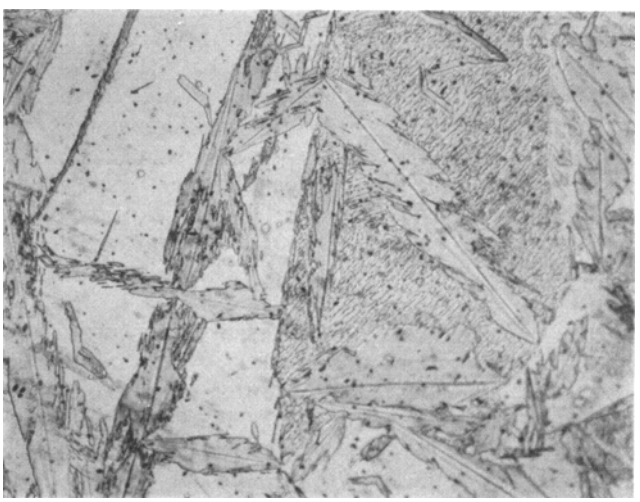

Enlarged View of Martensite Plates

Fig. 3 — An enlarged view of martensite plates in Fe-30 wt pct Ni alloy. The microstructure after the burst at −15 °C shows the penetration of some martensite plates to the midrib region of other plates and the irregular interface between martensite and austenite. Magnification 292 times.

An enlarged view of martensite plates formed after the burst is presented in Figure 3 to illustrate an interesting feature of martensitic growth. The micrograph shows that some plates penetrate to the midrib region of earlier formed plates, and the deepest penetration at a junction is always made by the midrib trace. These plates are presumably formed during the same burst. The penetration implies that the midrib is the first portion of the plate to form, and the growth rate of lateral thickening of the plate is substantially slower than that of the midrib expansion. Patterson and Wayman[24] also observed this penetration phenomenon in an Fe-32 pct Ni alloy and showed clearly that the later-forming plate penetrates to the boundary of the twinned region of the pre-existing plate. In addition, they have investigated the effect of composition on the extent of internal twinning in Fe-Ni alloys containing 29.8 pct, 32.0 pct, and 33.2 pct nickel, respectively, showing the increasing extent of twinning in the midrib region and the trend toward a straighter austenite-martensite interface with increasing nickel content. They also confirmed that the untwinned region of a martensite plate contained densely tangled dislocations, indicating that the shear process became slip instead of twinning.

From the above analysis, one can further infer that the growth of the partially twinned martensite plates consists of two stages. The first stage involves the formation of the midrib plane by twinning, whereas the second stage involves the lateral thickening by slip. In accord with Nishiyama's classification of the fast and intermediate velocity regimes of martensitic growth, the growth rate of radial expansion of the midrib region is much faster than that of the lateral thickening by at least an order of magnitude. As will be seen shortly, both acoustic emission and magnetic methods used in the present investigation are *velocity*-sensitive techniques. The amplitude of detected signals in both methods is proportional to the square of the growth velocity of martensite plates. Therefore, the transformed volume responsible for the detected AE and magnetic signals is not the total volume of a martensite plate. In the light of the two-stage growth process, it is reasonable to deduce that the quickly expanding midrib region is the principal source for the signals detected by velocity-sensitive measurements, while the slowly thickening region presumably makes only a small contribution to the signals. Furthermore, in the Fe-30Ni alloys investigated in the present study, the thickness of the twinned region in a martensite plate is relatively thin and surrounded by a large thickening region on both sides that forms later.[24] The ratio of the mean semithickness to the mean radius of martensite plates is known to be around 0.11 to 0.05.[25] The ratio of the thickness of the midrib region to the other two dimensions is then expected to be even smaller. All these facts provide grounds for us to assume that the disc-shaped midrib region is the only source for signals detected in AE and magnetic measurements. Since the rate of change of the midrib thickness is negligible compared to the radial growth of a plate, we can further assume, for simplicity, that the source is a radially expanding circular disk with an approximately constant thickness. The circular source model will be used in analyses of both AE and magnetic signals throughout this paper.

IV. ACOUSTIC EMISSION MEASUREMENTS

A. *Brief Overview*

Various processes involving a sudden release of strain energy in materials are often accompanied by acoustic emission (AE). Acoustic emission signals are observed in plastic deformations, crack growth, and many rapid structural changes. Since AE signals carry information on the source mechanism and its time history, it is feasible to utilize the AE technique in studying the growth dynamics of martensitic transformations. However, some previous applications of AE technique to martensitic transformations were only successful in relating the AE count number to the fraction of the transformed volume.[26,27] In general, most applications of AE technique have been limited to a qualitative level over the years. Until recently, few attempts were made to analyze AE signals quantitatively for source characterization.[28,29] The advent of newly designed linear transducers[30,31] now makes quantitative AE analyses possible. A linear piezoelectric transducer developed by the National Bureau of Standards (NBS)[31] has been used in the present study.

Acoustic emission signals emanating from various deformation processes are of a broadband nature. The measuring frequency range of these AE signals extends from tens of KHz up to tens of MHz. In order to characterize the source behavior of a growing martensite plate from the detected AE signals with such a wide spectrum, the linear frequency response of the transducers and the signal processing devices is undoubtedly important for a quantitative analysis. Much previous effort has been devoted to this subject. However, the frequency response of the propagation media that the AE signals pass through has been an ignored feature. It is well established that the ultrasonic attenuation caused by grain boundary scattering in polycrystalline materials is strongly frequency dependent.[32,33] Therefore, the broadband AE signals undergo a considerable distortion when they pass through the medium. The nonlinear behavior of the media has not been adequately treated in the previous quantitative AE analyses,[28,29] in which the transfer function of the media has been simply taken to be a Green's function. It should be noted that the Green's function formalism assumes a linear frequency response and only takes care of spatial attenuation. Obviously, a quantitative AE analysis would be of little meaning without a proper handling of the signal distortion caused by the frequency-dependent media attenuation.

It is very time consuming and tedious to accurately measure the frequency response of a material over a wide frequency range. As an alternative, an engineering approach to deal with media attenuation is used in the present study. The detailed theory and applications of this method are given elsewhere.[34] This approach combines spectral analysis with the analysis of real-time signals. Some carefully chosen quantities, such as the first node frequency and the peak time, are used for AE source characterization. The node frequencies represent a series of minima in the frequency spectrum when the first arriving P-wave pulse is Fourier transformed. The peak time is the time interval for the P-wave pulse to reach its peak value. Both the first node frequency and the

peak time are found to be least sensitive to the media attenuation. This property enables us to circumvent the media distortion and directly infer major source parameters such as the final size and the average velocity of martensitic growth.

B. *Experimental*

1. *Specimen preparation*

An Fe-30 wt pct Ni alloy was melted in an induction furnace with argon atmosphere, and rods of 9.5 mm in diameter and 100 mm in length were cast in the furnace. After the homogenization treatment at 1200 °C for 170 hours, the rods were swaged to 3.63 mm in diameter through several passes and finally cut into discs of 1-mm thickness. Another Fe-40 wt pct Ni alloy was prepared by a similar procedure, and rods (18 mm in diameter and 100 mm in length) were cut into pieces of 10-mm length. The 40 wt pct Ni alloy was chosen for the acoustic transmission medium, because it closely matched the 30 wt pct Ni alloy elastic constants but does not transform martensitically.

The specimen is designed to be conical, with the source region being restricted to the apex of the cone. Diffusion bonding was used to eliminate the interface separation between the two parts of different compositions in order to prevent possible wave reflections at the interface during AE measurements. To accomplish this, a small disc of Fe-30 pct Ni alloy was first attached to a larger section of Fe-40 pct Ni alloy with the contact surfaces of both parts being polished and cleaned beforehand. The two parts were then pressed together in a hydraulic press, and a clamp was attached. The clamped specimen was vacuum encapsulated and heat treated in a furnace at 1150 °C for 100 hours so that the voids along the interface between the two sections totally disappeared and the grains along the interface grew into each other, as verified by metallographic observations. Finally, the specimen was machined to the required conical shape and dimensions, which are illustrated in Figure 4. All the specimens were austenitized at 900 °C for 4 hours and then water quenched before the experiment. The average grain diameter in the whole specimen was found to be 0.25 mm.

2. *Experimental setup*

A schematic diagram of the experimental setup is shown in Figure 5. An NBS piezoelectric transducer was used in the present study. The transducer, which provides a voltage linearly proportional to vertical displacement only, was placed at the center of the basal plane of the specimen, namely, at the epicenter position, with a thin layer of vacuum grease in-between to ensure a good contact. The distance between the source region and the transducer was about 10 mm. Although the source plane of a martensite plate may be oriented randomly at the apex of the specimen, this layout greatly simplifies the analysis of AE signals, because directly arriving P waves only cause vertical displacement at the epicenter position and direct S waves will not be detected by the transducer, which only senses vertical movement. Reflected S waves, as well as reflected P waves, may be detected, but they are well separated from the first arriving P wave by a time span. Therefore, the analysis can focus on the first motions due to direct P waves.

The specimen and the transducer were placed inside a glass Dewar which, in turn, was placed inside a cooling Dewar filled with liquid nitrogen. As the temperature was lowered to the transformation range, the growth of martensite plates produced a series of AE signals. The frequency response of the NBS piezoelectric transducer is known to be flat up to 1.5 MHz and gradually falls off to zero at about 5.5 MHz.[35] This provides another source of frequency-dependent attenuation. The combined effect of two attenuation factors (the medium and the transducer) on the AE signals is that only large transformation events can be detected.

The NBS transducer was connected with a two-stage wideband preamplifier. The first stage was a field effect transistor (FET) linear voltage follower (OEI 9963), and

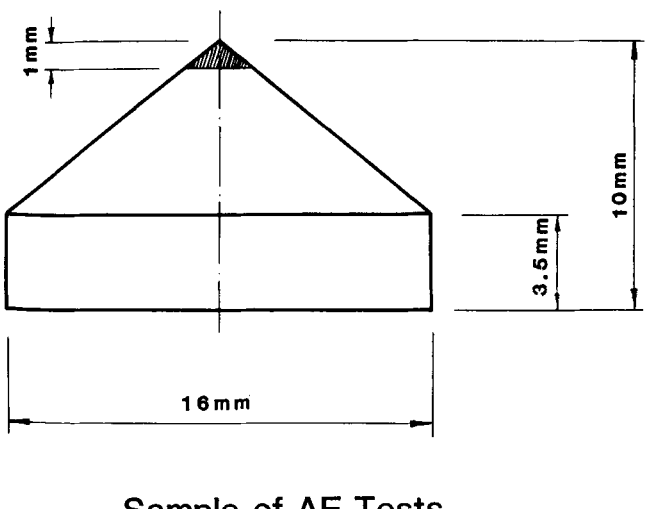

Fig. 4—Conical specimen of AE measurement. The shaded region at the apex of the cone is made of Fe-30 wt pct Ni, while the rest of the specimen is Fe-40 wt pct Ni.

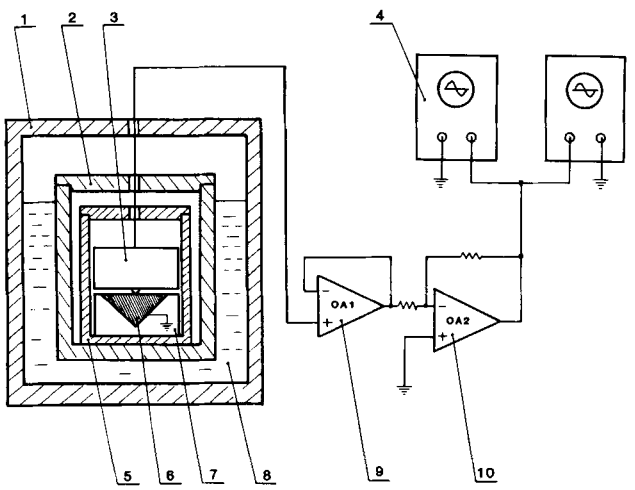

Fig. 5—Schematic diagram of the AE experimental setup: (1) liquid nitrogen Dewar; (2) glass Dewar; (3) NBS linear transducer; (4) fast storage oscilloscope; (5) brass shielding enclosure; (6) conical specimen; (7) epoxy mount; (8) liquid nitrogen coolant; (9) FET linear voltage follower; and (10) operational amplifier as an inverter.

the second stage was a wideband operational amplifier (OEI 9914A). Piezoelectric transducers are known to have very high output impedance. To obtain a satisfactory impedance matching, a FET linear voltage follower was used to serve as an impedance buffer. The wideband operational amplifier was connected as an inverter. The preamplifier gave a total gain of 30 db and a bandwidth from 30 KHz to 30 MHz. The low frequency rolloff was adjusted to eliminate environmental mechanical noises.

The output of the preamplifier was then fed into two parallel connected Tektronix fast storage oscilloscopes (Tektronix 7834 and 7623A). Since the surface displacement caused by a P wave can be either upward or downward depending on the source orientation, two oscilloscopes were set on opposite triggering polarities in the storage mode to ensure that the first motion of P waves would be detected and recorded by one of the oscilloscopes. The bandwidths of the oscilloscopes were from 0 to 400 MHz for the Tektronix 7834 and from 0 to 100 MHz for the Tektronix 7623A. When a signal was recorded by both oscilloscopes, a comparison was made between the two signal patterns to determine the first motion in a series of pulses. Afterward, the photo records of the stored analog signals were converted to digital signals by a digitizer for further analysis.

The electrical characteristics of the equipment used in the present study (including that for the magnetic measurement) are summarized in Table I. The wide bandwidths of the required equipment often bring about annoying noise problems that limit the use of high gain in signal amplification. With the bandwidths used in our study, FM radio interference sometimes became very annoying and hard to eliminate. It was found that perfect shielding and common grounding for each apparatus were helpful to reduce the noise level. In addition, all connecting leads and cables were made as short as possible.

C. *Results and Analysis*

Once the specimen is cooled down to the transformation temperature range, AE signals due to the formation of martensite can be frequently recorded by the storage oscilloscopes. Different signal patterns have been observed at different temperature ranges, which we refer to as preburst, burst, and postburst.

The first burst in the AE specimens occurs at about −30 °C. Only a very few signals have been detected above the M_b temperature. These preburst signals, as shown in Figure 6(a), have their first motion, namely, the first arriving P wave, well separated from the subsequent reflected waves that appear as a series of oscillations. The preburst signals have a relatively simple pattern, and they

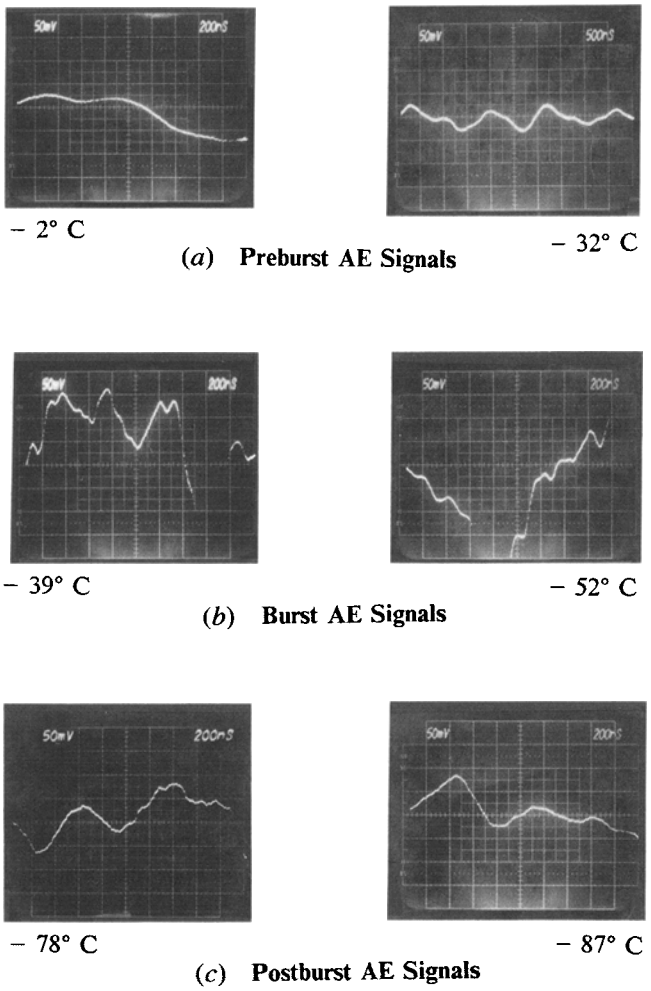

Fig. 6—Recorded AE signals at different temperatures: (*a*) preburst signals recorded at −2 °C (left) and −32 °C (right); (*b*) burst signals recorded at −39 °C (left) and −52 °C (right); and (*c*) postburst signals recorded at −78 °C (left) and −87 °C (right). Time scale is 200 ns/div (except 500 ns/div for the right one in (a)). Voltage scale is 50 mV/div measured at the output end of the preamplifier.

are most likely to represent the formation of single martensite plates, which supposedly have not yet gained enough driving force to trigger the formation of other neighboring plates.

The burst phenomenon usually lasts over a temperature range of 20 to 25 deg. Some of the burst signals are shown in Figure 6(b). The burst signals display a more complicated pattern; *i.e.*, their first motion involves a number of overlapping single pulses. They usually appear to be shower-like and choppy, forming a long rising

Table I. Characteristics of the Electronic Equipment Used

	Operational Amplifier Type 9963	Operational Amplifier Type 9914A	Oscilloscope Type 7834	Oscilloscope Type 7623A
Manufacturer	Optical Electronics Inc.	Optical Electronics Inc.	Tektronix Inc.	Tektronix Inc.
Bandwidth	dc to 30 MHz	dc to 200 MHz	dc to 400 MHz	dc to 100 MHz
Gain	0 dB	30 dB	—	—
Used for	AE measurement only	magnetic and AE measurements	magnetic and AE measurements	AE measurement only

voltage ramp. The burst signals obviously represent multievents as a result of an autocatalytic avalanche.

After the burst region is passed, the shower-like burst signals gradually disappear and are replaced by a simple signal pattern. The postburst signals are very similar to the preburst signals, as shown in Figure 6(c). Since 60 to 70 pct of the original austenite has already transformed to martensite after the burst region, the grains are partitioned by many large martensite plates which build up severe strain conditions in the small retained austenite segments. As a result, the probability for autocatalytic formation of plates becomes very slim. Thus, it is fair to say that the postburst signals also represent the formation of single martensite plates.

Since many individual events overlap in the burst signals which make it extremely difficult to analyze the signals with any accuracy, we will concentrate on the single events in the preburst and postburst regions to extract quantitative information on the growth velocity. It is worth mentioning that the characteristics of the preburst, burst, and postburst signals described above are displayed more clearly by the magnetic measurements of the same transformation, because the magnetic signals show very simple patterns and are easy to distinguish between single events and multievents.

The signal analysis follows the approach described in Reference 34. In brief, the first arriving P-wave pulse of the transformation event is Fourier transformed to obtain an amplitude spectrum in the frequency domain, in which a series of minima called nodes can be found. The positions of these nodes are insensitive to the media attenuation, and the frequency of the first node may be chosen to characterize the source events. The nodes are a result of the interference of the wavelets emitted by different parts of the finite size source. The node frequencies have been shown to be closely related to the final size of the source. For circular disc source events such as are assumed in the present study, the first node frequency is a function of the final radius of the source and its orientation with respect to the detector, namely, the takeoff angle. It is found in our study that for a fixed takeoff angle, there is a one-to-one correspondence between the first node frequency and the final radius of the martensite plate when the source expansion velocity ranges from 0 to 0.6 v_t, where v_t is the shear wave velocity of the medium. This range covers most of our interest, and, beyond that, relativistic effects result in some deviation. In principle, the takeoff angle can be determined by multitransducer measurements. However, for the single transducer measurements performed, by choosing only the strongest AE signals for further analysis, we have selected those signals which must have a takeoff angle close to the maximum probability direction, because the amplitude of the signals drops steeply when their orientations deviate from it.[34] After the final radius is determined from the first node frequency of an AE signal, the growth velocity can be calculated from the obtained plate size and the peak time of the AE signal in the real-time domain.

The calculated values of the final size and the average growth velocity for individual events detected at different temperatures are listed in Table II and plotted in Figure 7. It is found from our AE measurements that the growth velocity of individual transformation events

Table II. Calculated Results of AE Signals

Temperature (°C)	Node Frequency (MHz)	Peak Time (μs)	Radius (mm)	Velocity Ratio
−12	3.17	0.36	0.68	0.51
−32	4.15	0.35	0.52	0.42
−40	1.47	0.52	1.50	0.68
−48	3.47	0.50	0.62	0.37
−56	4.15	0.35	0.52	0.42
−58	1.95	0.49	1.12	0.58
−58	5.16	0.31	0.42	0.39
−60	2.54	0.42	0.86	0.55
−70	5.04	0.40	0.43	0.33
−70	2.59	0.53	0.84	0.45
−72	5.47	0.38	0.39	0.32
−72	5.04	0.31	0.43	0.40
−76	4.15	0.35	0.52	0.42
−78	3.76	0.33	0.58	0.48
−78	3.91	0.21	0.55	0.64
−78	4.00	0.48	0.54	0.34
−80	6.30	0.16	0.34	0.56
−82	8.98	0.16	0.24	0.43
−82	5.08	0.50	0.43	0.27
−87	4.64	0.44	0.47	0.32
−89	3.22	0.36	0.67	0.50
−97	6.25	0.33	0.35	0.32

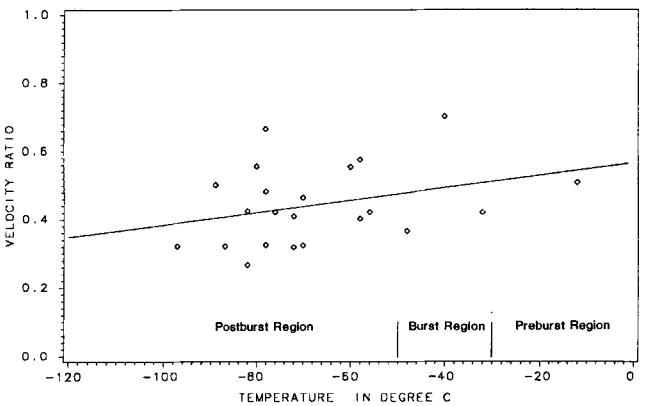

(*a*)

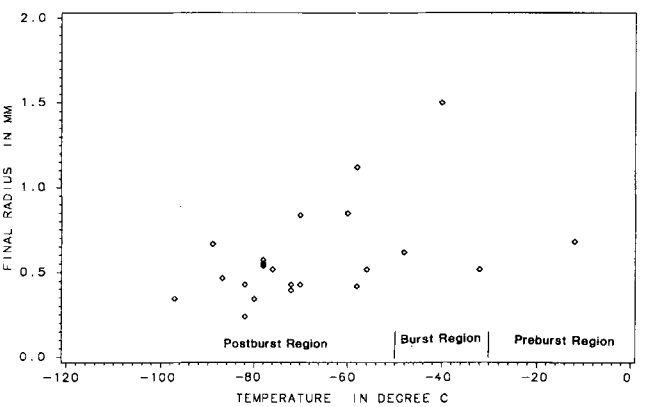

(*b*)

Fig. 7—Diagram of derived source parameters: (*a*) velocity ratio v/v_t *vs* temperature and (*b*) final radius *vs* temperature. The takeoff angle θ is assumed to be 55 deg.

varies from 0.25 to 0.65 in terms of the velocity ratio (v/v_t), where v_t = 2.77 km/s[36] is the shear wave velocity in an Fe-30 pct Ni alloy. The ratio of the maximum to minimum growth velocities is nearly 3:1, and there is perhaps a slight decrease of the growth velocity as temperature falls, indicated by the linear regression fitted line in Figure 7(a). The decrease in the final size of martensite plates with falling temperature is quite obvious in Figure 7(b). Because of the relatively severe frequency-dependent attenuation imposed by both the media and the transducer, high-frequency AE transformation signals (namely, very short pulses) are diminished too much in amplitude to be detectable. This is probably why the average final size of martensite plates being detected (Figure 7(b)) is found to be greater than the average grain diameter.

V. MAGNETIC INDUCTION MEASUREMENTS

A. *Basic Principles*

In the martensitic transformation of Fe-Ni alloys, the structural change from weakly ferromagnetic austenite (fcc lattice) to strongly ferromagnetic martensite (bcc lattice) involves a drastic change in magnetization. According to Lenz's law, the change in magnetization in an Fe-Ni specimen creates an electromotive force (emf) or a voltage in a coil of wire surrounding the specimen. This emf is proportional to the time rate of the local change of the magnetic moment ΔM as

$$E = -\frac{d\Phi}{dt} \propto \frac{d(\Delta M)}{dt} \qquad [1]$$

where E is an instantaneous voltage in the circuit and $d\Phi/dt$ is the time rate of change of the magnetic flux through the circuit. This induced voltage carries useful information about the martensitic transformation. Assuming that a strong saturation magnetic field is applied parallel to the axis of a specimen, the magnetic domains in austenite are totally oriented along the direction of the magnetic field. A small region of austenite is then transformed to martensite, accompanied by a sudden increase of magnetization in the same direction. The local change of the magnetic moment ΔM due to the martensitic transformation is directly related to the corresponding volume of the martensitic product V by

$$V = \frac{\Delta M}{\Delta I_s} = \frac{\Delta M}{I_s^\alpha - I_s^\gamma} \qquad [2]$$

where I_s^α and I_s^γ are the saturation intensities of magnetization in martensite and austenite, respectively. Therefore, the induced voltage in a coil wound around the specimen is proportional to dV/dt, the time rate of change of the transformed volume.

Based on the circular disc source model with a constant thickness, the volume in Eq. [2] is written as

$$V = \pi R^2 h \qquad [3]$$

where R is the radius of the martensite plate and h is the thickness of the midrib region. Combining Eqs. [1] through [3], one can derive that

$$E = CR\frac{dR}{dt} = CRv \qquad [4]$$

where C is a proportionality constant and v is the average growth velocity. Taking the time derivative of the induced voltage, the slope of the voltage signal is given by

$$\frac{dE}{dt} = Cv\frac{dR}{dt} = Cv^2 \qquad [5]$$

Under the assumption of a constant growth velocity, the induced voltage is linear in time, with the slope proportional to the square of the growth velocity, and the magnetic induction method is indeed velocity-sensitive. Most recorded signals of single events show a linear rising slope, which seems to support this model.

B. *Experimental*

1. *Specimen preparation*

The original materials in this experiment were 99.99 pct pure iron and nickel. An Fe-30 wt pct Ni alloy was melted in an induction furnace under an argon protective atmosphere, and rods (9.5 mm in diameter and 100 mm in length) were cast in the furnace. The rods were then homogenized at 1200 °C for 48 hours to eliminate the columnar casting structure and obtain nearly equiaxial grains. After the homogenization treatment, the rods were cut into cylinders of 9.5 mm in diameter and 15 mm in length. The cylinders were further machined to be hollow with a wall thickness of 1.25 mm in an attempt to reduce the effect of eddy current on the magnetic signals. (As will be seen later, even with the hollow specimen, eddy currents still play a significant role in the shape of the signals.) Then, specimens were austenitized at 900 °C for four hours and water quenched. All the heat treatments were performed with specimens encapsulated in quartz tubes with a vacuum of 10^{-7} torr. At room temperature, the specimens remained as nearly 100 pct austenite. The average grain size was found to be 0.2 mm.

2. *Experimental setup*

A schematic diagram of the experimental setup for the magnetic measurements is shown in Figure 8. A dc magnet was used to produce a uniform 8000 Oersted magnetic field which is strong enough to saturate the specimens in either austenite or martensite states. A cylindrical specimen of Fe-30 pct Ni alloy was placed between two poles of the magnet with its axis parallel to the direction of the field. A detection coil was tightly wound around the specimen. Both specimen and coil were placed in a copper enclosure which was proven to be essential for shielding and prevention of external electromagnetic interference. The copper enclosure was wrapped inside a styrofoam sleeve which served as a heat insulator (not shown in Figure 8). The temperature variation required by the martensitic transformation was achieved by flowing a cooling gas through the enclosure. Nitrogen gas from a gas cylinder first passed through a spiral pipe immersed in a container filled with liquid nitrogen, then entered the enclosure, and finally left it. The cooling gas circulation resulted in a steady cooling rate. (The cooling rate may vary as desired by controlling the gas flow rate.) The detection coil was connected to a preamplifier and then to a high-speed storage oscilloscope.

Schematic Diagram Of
Experimental Set-up Of Magnetic Induction Method

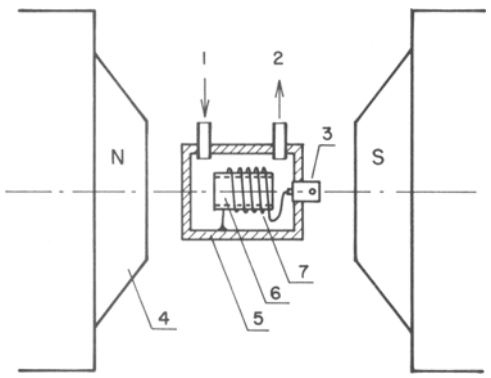

(1) Cooling gas inlet (N_2)
(2) Cooling gas outlet
(3) BNC Connector
(Connected with coaxial cable)
(4) Magnet (8000-gauss field)
(5) Copper shield
(6) Specimen (hollow)
(7) Pick-up coil

Fig. 8—Schematic diagram of the magnetic measurement: (1) cooling nitrogen inlet; (2) cooling nitrogen outlet; (3) BNC connector; (4) magnet (8000-gauss field); (5) copper shield; (6) hollow cylindrical specimen; and (7) detection coil.

To guarantee the least distortion in signals caused by the detecting and recording systems, wide bandwidths are extremely vital for every electronic apparatus. The magnetic measurement requires a flat frequency response from dc to some upper limit which must be much higher than the frequency range of the transformation signals. Many commercial high-frequency linear amplifiers often have a low-frequency rolloff which results in oscillations following the initial rise in the magnetic signals. The reason for these oscillations is that the decaying tail in magnetic signals due to the effect of eddy currents is of lower frequency and is distorted by the presence of the low-frequency rolloff. These oscillations make it virtually impossible to analyze the magnetic signals. The preamplifier chosen was an operational amplifier (OEI 9914A) connected as an inverter with a gain of 30 dB and a bandwidth from dc up to 200 MHz. The oscilloscope used to record signals was a Tektronix 7834 high-speed storage oscilloscope with a bandwidth from dc to 400 MHz. The response time of both the preamplifier and the oscilloscope was much faster than the time durations of the transformation signals (usually greater than 30 ns) so that virtually no distortion resulted from signal amplification and recording.

3. *Design of detection coil*

Intuitively, one would think that the sensitivity of the detection coil increases with the increasing number of turns of the coil. However, this is not true for the precision measurement of high-frequency signals. With the increasing number of turns N in the coil, the inductance of the coil L increases (proportional to N^2), which in turn raises the time constant of the coil τ ($\tau = L/R$, where R is the resistance of the coil). As will be shown by Eq. [12], when the time constant of the coil is much greater than that of the specimen, the amplitude of the induced signal E_{max} is proportional to N and is inversely proportional to τ. Therefore, increasing the number of turns would not improve the sensitivity. On the contrary, the greater the time constant of the coil, the worse the sensitivity of the coil is to the high-frequency transformation signals. We have systematically studied the effect of the number of turns of a coil on its time constant and high-frequency rolloffs by using a calibration coil as the primary coil. The rolloff here corresponds to the frequency at which the amplitude of the induced voltage starts falling. The results are summarized in Table III.

It becomes obvious now that the fast transformation signals would be severely distorted by the detection coil with a time constant much greater than that of the transformation event. Figure 9 shows some recorded transformation signals using a 600-turn coil, in which the very long decaying tails are the indication that signals evidently carry the characteristics of the detection coils. In order to eliminate the effect of the detection coil on the shape of induced signals, the time constant of the coil should be kept much smaller than that of the transformation events, which ranges from tens to hundreds of nanoseconds. It will be seen shortly that the precision measurement of the time constant of the transformation event τ_1 is crucial to the signal analysis. Even the time constant of a 20-turn coil (60 ns) seems inappropriate, because it would give rise to a considerable error in measuring τ_1. The actual detection coil used in our experiment was a 3-turn coil, and its time constant was estimated to be about 1.35 ns. By doing so, the effect of the detection coil on the signal shape has been minimized.

C. *Effect of Eddy Currents*

Based on Eqs. [1] through [5], the variation of ΔM and E with time are plotted by solid curves in Figure 10.

Table III. Characteristics of Detection Coils

Number of Turns	Time Constant (ns)	Rolloff Frequency (MHz)
20	60	17.5
40	250	6.0
100	1800	1.5
600	50,000	0.5

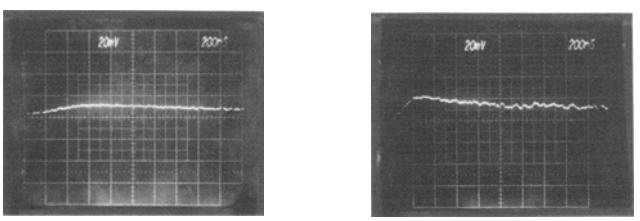

(*a*) – 67° C (*b*) – 39° C

Distorted Transformation Signals Using a 600-turn Coil

Fig. 9—Distorted transformation signals using large-turn coils. Signals in (*a*) and (*b*) were measured using a 600-turn coil. Time scale is 200 ns/div. Voltage scale is 20 mV/div.

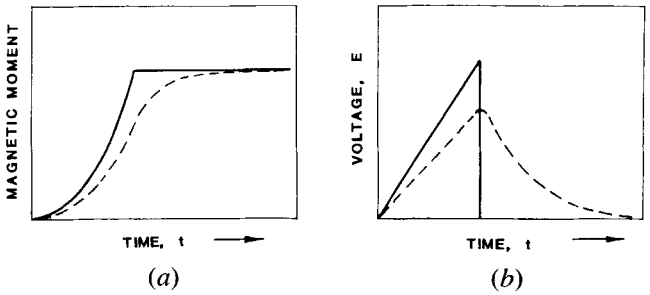

Fig. 10—Variation of magnetic moment and voltage with time: (*a*) ΔM-t curve and (*b*) E-t curve. The solid curves represent the ideal cases without the effect of eddy currents, and the broken curves represent the actual cases with eddy currents in effect.

These curves represent an ideal case, where no eddy current effects of the specimen have been taken into account. In reality, the amplitude and form of the induced voltage pulses are markedly influenced by the rate of change of induction in the specimen, which, in turn, is controlled by the decay of the eddy currents set up in the specimen. Eddy currents can be understood in terms of Lenz's law, since the specimen is a good conductor which can be considered as a coil itself. Therefore, any local change in magnetization will create eddy currents inside the specimen to oppose this change. From a theoretical point of view, a local change in magnetization causes the change of induction B, and the rate of change in B is governed by the equation for the propagation of this change as a function of position and time. The change in induction is retarded by the presence of eddy currents during its propagation from the source to the windings of the coil. In general, the effect of eddy currents is to reduce the amplitude of the induced voltage and to create a decaying tail to oppose the sudden end of the change in magnetization. The ΔM-t and E-t curves under the influence of eddy currents are presented as broken curves in Figure 10. In addition, the extent to which the induced voltage signals are influenced by eddy currents depends on how far the source of local magnetic change is from the coil windings.

The effect of eddy currents on the induced voltage in a detection coil has been studied in several papers devoted to the Barkhausen effect.[37,38] Tebble *et al.*[37] have given a detailed mathematical treatment on the decay of induction accompanying a local change in magnetization in a cylindrical specimen. They proposed that the influence of eddy currents can be represented by an effective time constant for the source, which turns out to be a very useful tool to analyze magnetic signals. Note that the time constant of a magnetic source is associated with the specimen and should not be confused with the time constant of the detection coil discussed in the previous section.

It is clearly shown in Tebble's paper that both the amplitude and the shape of the induced voltage depend heavily on the spatial location of a change in magnetization. The voltage amplitude becomes smaller and the subsequent decaying tail longer as the ratio b/a decreases, where a is the radius of a cylindrical specimen and b is the distance of an event from the axis of the cylinder. The time constant of a magnetic event is then defined as the time duration when the change in flux or the induced voltage falls to $1/e$ of its maximum value. Depending on the location of a source event, the time constant τ_1 decreases from its maximum value (at the axis of the cylinder) to zero (at the surface), as b/a increases from zero to one. When hollow cylindrical specimens are used, the effect of eddy currents is reduced to some extent, but the same principle applies; *i.e.*, the time constant reduces to zero, and the voltage amplitude reaches a maximum as a source approaches the outer surface of the hollow cylinder. In fact, the effective time constant of a transformation event can be measured directly from the decaying tail of the recorded voltage signal. The important fact to be kept in mind is that the time constant of an event provides useful information on how deeply it is located from the surface (or, more accurately, how far it is from the windings of the coil).

In regard to the disc-shaped source in our study, the time constant τ_1 at different portions of the disc varies when the disc plane is not parallel to the axis of the specimen. Since the size of a martensite plate is much smaller than that of the specimen, the variation of τ_1 with the changing depth of a martensite plate in the specimen is approximately linear. Therefore, the effective time constant of a plate may be taken to be that at its center, regardless of its orientation. It will be shown in the method of signal analysis that the time constant of each transformation event needs to be known accurately in order to calculate its growth velocity. This also explains why the time constant of the detection coil should be kept as small as possible without causing any error in measuring the time constant of transformation events.

The following test has been carried out to investigate the localization of magnetic signals in our experiment. The transformation signals were measured using two closely spaced 3-turn coils, which were tightly wound around the specimen separately. The distance between the two coils was only 2 mm. Each coil was 9.5 mm in diameter and 1.8 mm in length. The two coils were connected to two independent preamplifiers of the same gain (30 dB) which controlled the horizontal and vertical beam reflection of the storage oscilloscope, respectively. The storage oscilloscope was set up in the X-Y display mode and was triggered by one of the coils, for example, by the vertical (Y) deflection only. If a magnetic signal was detected by both coils, the signal trace recorded by the oscilloscope would have both X and Y components. As a matter of fact, almost all the signals recorded during the experiment showed a deflection in the Y direction only, except one caught right at the M_b temperature which had some scattered features. This was probably because the burst involved the formation of many martensite plates over a relatively large volume which evidently affected both coils. This result implies that the magnetic signals detected by a coil come only from those events that take place in the very close vicinity (<1 mm) of the coil windings.

D. *Results*

Because of the simple signal patterns, the magnetic signals can be easily classified as preburst, burst, and postburst according to the corresponding temperature

ranges. The first burst, *i.e.*, the M_b temperature, in the magnetic specimens occurs at about −15 °C. Very few signals were recorded above M_b, which appeared as single pulses rising quickly to its peak and then decaying gradually to zero, as shown in Figure 11. They are most likely to represent the formation of single martensite plates. As temperature reached the burst region, many large, shower-like signals were recorded which appeared very choppy, high-amplitude, and long-lasting. Different types of burst signals are presented in Figure 12. Each individual ripple or pulse in the burst signals presumably represents the formation of a single martensite plate with the rising time ranging from 20 to 80 ns. These signals obviously represent multievents as a result of an autocatalytic avalanche. The postburst signals show the same pattern as that of preburst ones. Figure 13 shows some postburst signals that all have a short rising part followed by a relatively long decaying tail. The amplitude of the rising part and the length of the decaying tail in these signals vary from each other. The time duration of the rising part (termed the peak time) of all single pulses ranges between 25 and 100 ns. The time constant of these single pulses, τ_1, extends from 30 to 300 ns. The varying lengths of the decaying tails in these single pulses, as well as their amplitudes, indicate the different depths from the coil windings at which the martensite plates form.

In short, the signal patterns at different temperature ranges lead to the conclusion that the transformation signals above and below the burst temperature region correspond to single events, whereas the signals within the burst region are related to multievents. Again, our analysis will be focused only on the single events to derive the growth velocity of individual martensite plates.

E. *Signal Analysis*

It is known from Eq. [5] that the growth velocity can be deduced from the rising slope of the induced voltage. However, the amplitude of the recorded voltage E_{max} is reduced to some extent due to the effect of eddy currents. Thus, it is necessary to make a correction for E_{max} before Eq. [5] can be used.* In discussing the form of

*Strictly speaking, the peak time would be affected by eddy currents such that it would be, to some degree, longer than the actual time of formation of a plate. Since the peak time in single pulses is in the same order of magnitude as the measured time constant τ_1, the error caused by the effect of eddy currents on the peak time is believed to be negligible.

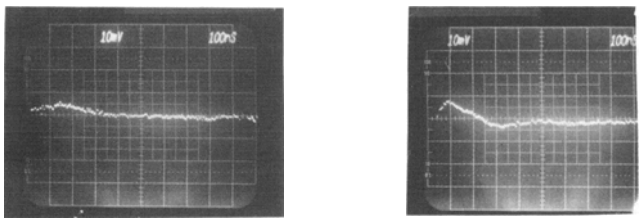

(*a*) − 6° C (*b*) − 14° C

Preburst Magnetic Signals of Martensitic Transformation

Fig. 11 — Preburst magnetic signals of martensitic transformation: (*a*) −6 °C and (*b*) −14 °C. The time scale is 100 ns/div and the voltage scale is 10 mV/div measured at the output end of the preamplifier.

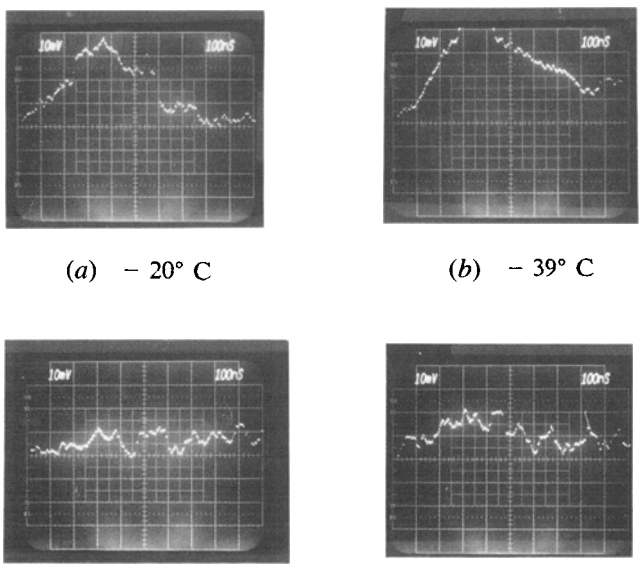

(*a*) − 20° C (*b*) − 39° C

(*c*) − 24° C (*d*) − 33° C

Burst Magnetic Signals of Martensitic Transformation

Fig. 12 — Burst magnetic signals of martensitic transformation: (*a*) −20 °C; (*b*) −39 °C; (*c*) −24 °C; and (*d*) −33 °C. The scales are the same as in Fig. 11.

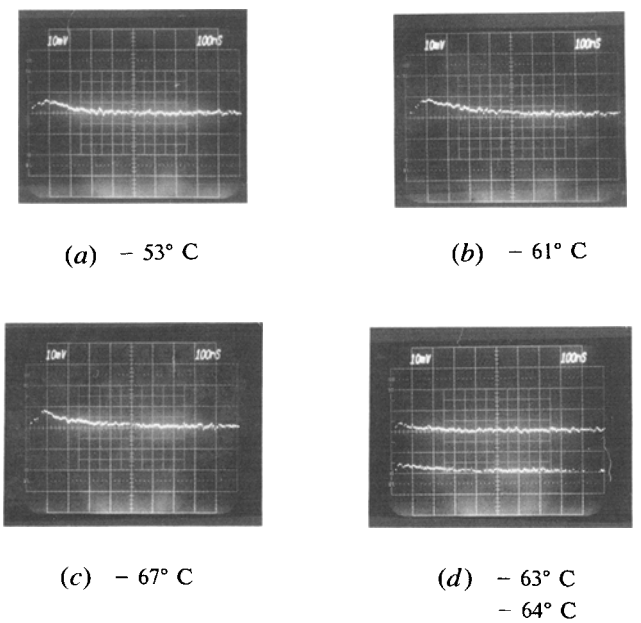

(*a*) − 53° C (*b*) − 61° C

(*c*) − 67° C (*d*) − 63° C
− 64° C

Postburst Magnetic Signals of Martensitic Transformation

Fig. 13 — Postburst magnetic signals of martensitic transformation: (*a*) −53 °C; (*b*) −61 °C; (*c*) −67 °C; and (*d*) −63 °C and −64 °C. The scales are the same as in Fig. 11.

the voltage pulses induced in a detection coil, Tebble *et al.*[37] proposed an ingenious idea to calculate the induced voltage. Their idea has been modified here to deal with the effect of eddy currents. Since the time constant τ_1 is related to the position of a magnetic event in the specimen, the specimen associated with a particular magnetic event can be considered as a single-turn coil with induction L_1, cross-section A_1, circuit resistance R_1, and the time constant $\tau_1 = L_1/R_1$. Imagine that a local change in magnetic moment ΔM results in a change in current i_1 through this "coil" according to the relation

$$\Delta M = i_1 A_1 \qquad [6]$$

The specimen and the detection coil can now be replaced by two coupled circuits of mutual inductance M, with the specimen as the primary coil and the detection coil as the secondary one whose time constant $\tau_2 = L_2/R_2$. Furthermore, the theory of coupled coils can be applied. The current induced in the secondary coil by a change in current i_1 in the primary is given by[39]

$$i_2 = \frac{Mi_1}{R_2} \frac{\alpha^2 - \beta^2}{2\beta} e^{-\alpha t}(e^{+\beta t} - e^{-\beta t}) \qquad [7a]$$

with

$$\alpha = \frac{\tau_1 + \tau_2}{2\tau_1\tau_2(1 - k^2)}$$

$$\beta = \frac{[(\tau_1 - \tau_2)^2 + 4k^2\tau_1\tau_2]^{1/2}}{2\tau_1\tau_2(1 - k^2)} \qquad [7b]$$

where $k = M/\sqrt{L_1 L_2}$ is the coefficient of coupling. It can be derived that with $k = 1$ (perfect coupling), i_2 takes the form

$$i_2 = \frac{Mi_1}{R_2}\left(\frac{1}{\tau_1 + \tau_2}\right) \qquad [8]$$

It has been shown that the detection coil is designed such that it has no effect on the shape of the induced pulse, *i.e.*, $\tau_1 \gg \tau_2$. Under this condition, i_2 is further simplified as

$$i_2 = \frac{Mi_1}{R_2\tau_1} \qquad [9]$$

The mutual inductance between the two coils under consideration can be approximately expressed by[37]

$$M = \frac{2\pi N_2 A_1}{(l_2^2 + r^2)^{1/2}} \qquad [10]$$

where N_2 is the number of turns in the detection coil, l_2 is the half length of the coil, and r is the radius of the coil. Substituting Eqs. [6] and [10] into Eq. [9], one can obtain an expression for the amplitude of the induced voltage:

$$E^i_{\max} = i_2 R_2 = \frac{Mi_1}{\tau_1} = \frac{2\pi N_2 \Delta M}{\tau_1(l_2^2 + r^2)^{1/2}} \quad \text{when } \tau_1 \gg \tau_2 \qquad [11]$$

It can be seen from Eq. [11] that the amplitude of the induced voltage is inversely proportional to τ_1, the value of which depends on the position of a source event in the specimen. When the source is on the surface of the specimen and underneath the coil windings, $\tau_1 = 0$. This is another extreme case where $\tau_1 \ll \tau_2$. A similar derivation leads to the following equation:

$$E^s_{\max} = \frac{Mi_1}{\tau_2} = \frac{2\pi N_2 \Delta M}{\tau_2(l_2^2 + r^2)^{1/2}} \quad \text{when } \tau_1 \ll \tau_2 \qquad [12]$$

This case implies that the amplitude of the induced voltage depends entirely on the time constant of the detection coil, while the specimen has no effect on the shape of the magnetic signals at all.

Combining Eqs. [11] and [12], one can easily obtain

$$E^s_{\max} = E^i_{\max}\frac{\tau_1}{\tau_2} \qquad [13]$$

where $E^s_{\max}$ and $E^i_{\max}$ are the amplitudes of the induced voltage for a source event at the surface ($\tau_1 \ll \tau_2$) and inside the specimen ($\tau_1 \gg \tau_2$), respectively. Since $E^i_{\max}$ and τ_1 can be measured from a recorded signal and τ_2 can be calibrated experimentally, $E^s_{\max}$ for each signal can be calculated from Eq. [13]. This enables us to remove the effect of eddy currents as if all the transformation events were moved to the surface underneath the detection coil. Therefore, all the recorded signals can be compared under the same conditions after such a correction has been made.

Now, we can use Eq. [5] and rewrite

$$\frac{dE}{dt} = \frac{E^s_{\max}}{t_p} = Cv^2 \qquad [14]$$

where t_p is the peak time corresponding to $E_{\max}$ and can be measured from a recorded signal. Once the growth velocity is known, the size of a martensite plate R (radius) is calculated by

$$R = vt_p \qquad [15]$$

However, the problem remains of determining the proportionality constant C in Eq. [14]. From Eqs. [2], [3], [12], and [15], one can derive the expression for C to be

$$C = \frac{2\pi^2 N_2 \Delta I_s t_p h}{\tau_2(l_2^2 + r^2)^{1/2}} \qquad [16]$$

It can be seen from Eq. [16] that the thickness of the disc source h is unknown, while other parameters are measurable. It is rather difficult to estimate this thickness, because there are no experimental data available so far to provide any quantitative estimate of the thickness of the midrib region. Thus, any calculated absolute values of the growth velocity based on this undetermined parameter would be of little significance. Nevertheless, the problem can be circumvented by the following treatment. Under the assumption of constant thickness, the relative values of the growth velocity of all recorded signals can be obtained according to Eq. [14]. Assuming the slowest growth velocity is 0.25 v_t, which corresponds to the slowest velocity observed in the acoustic emission measurements, we are then able to calculate the growth velocity of all signals recorded at different temperatures and the size of their corresponding martensite

Table IV. Calculated Results of Magnetic Signals

Temp. (°C)	Radius (μm)	Velocity Ratio	Temp. (°C)	Radius (μm)	Velocity Ratio
− 6	29	0.30	−62	39	0.35
−14	80	0.48	−63	62	0.45
−17	65	0.53	−63	67	0.32
−18	30	0.36	−63	38	0.46
−24	45	0.25	−64	47	0.57
−30	31	0.40	−64	74	0.38
−32	45	0.36	−65	107	0.31
−38	53	0.32	−66	81	0.42
−44	47	0.37	−67	50	0.33
−45	146	0.31	−67	80	0.48
−52	84	0.34	−67	107	0.45
−52	78	0.28	−68	46	0.56
−52	127	0.57	−68	96	0.41
−53	74	0.31	−70	39	0.36
−55	52	0.37	−71	52	0.29
−55	57	0.51	−71	46	0.37
−55	103	0.53	−72	78	0.35
−56	39	0.31	−73	38	0.34
−57	51	0.33	−74	57	0.33
−58	41	0.37	−74	49	0.36
−58	89	0.40	−75	64	0.27
−59	47	0.49	−76	62	0.41
−61	56	0.50	−78	30	0.36
−61	133	0.48	−81	48	0.25

plates using Eq. [15]. The results are presented in Table IV and Figure 14. Note that the growth velocities are given in terms of the velocity ratio v/v_t. The temperatures of recorded signals extend from −6 °C to −81 °C. The general trend found in Figure 14 is that as the temperature drops, the final radius of martensite plates decreases and the growth velocity slightly reduces but shows sizable scattering. The ratio of maximum to minimum growth velocities is nearly 2.5:1.

It is worth mentioning that an alternative to the assumption of constant thickness is to use the assumption of constant aspect ratio, in which the ratio of the thickness to the diameter of a martensite plate is kept constant during growth. Then, the absolute value of the final size of a plate could be determined by using a given aspect ratio, with the growth velocity calculated by Eq. [15]. When the aspect ratio of 1:25 was used, the results showed even greater scatter in growth velocity, namely, the ratio of maximum to minimum velocities was about 4:1.

VI. DISCUSSION

In the present study, quantitative analyses have been made for fast martensite growth events in an Fe-30 pct Ni alloy based on the experimentally measured magnetic and acoustic emission signals over a wide temperature range. The signal patterns indicate that the transformation can be divided into three categories according to the temperature ranges: preburst, burst, and postburst transformation regions. An accurate analysis can be made only for single transformation events that take place in the preburst and postburst regions.

Because the magnetic and acoustic emission methods are both velocity-sensitive in principle, very few signals

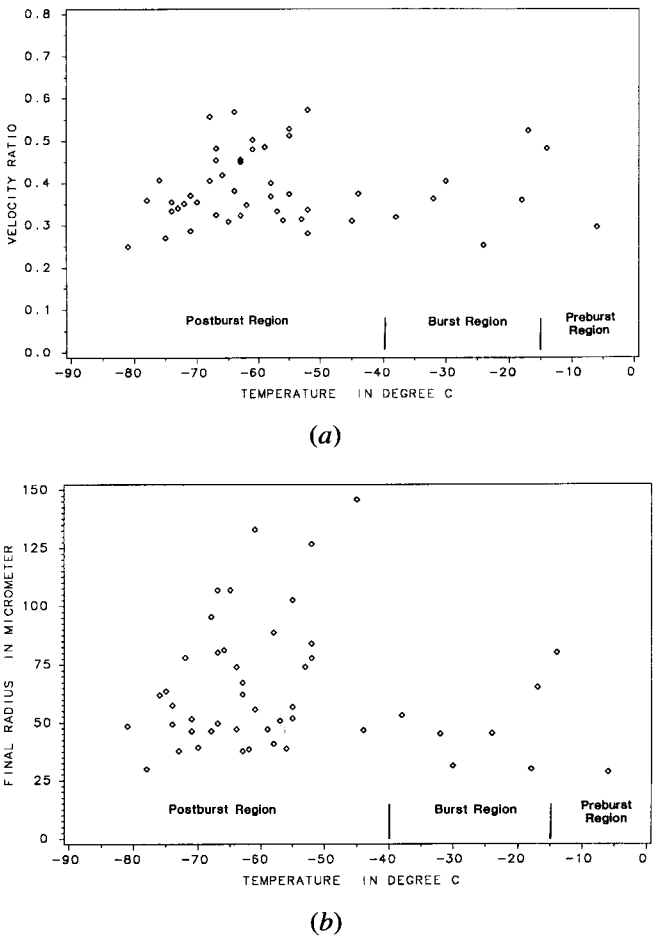

Fig. 14 — Calculated growth velocity and final size of single events: (*a*) velocity ratio *vs* temperature and (*b*) final radius *vs* temperature.

have been detected in the preburst region, and they all happened just above the M_b temperature. That the martensite plates formed above M_b were hard to detect by our measurements may result from two factors. First, these transformation events are probably too small, putting the intensity of these signals below the sensitivity of the detecting circuit. Second, it is more likely that a martensite plate formed above room temperature grows at relatively low velocity, so that it generally will not be detected by velocity-sensitive methods. Following Nishiyama *et al.*'s analytical treatment of martensitic growth,[40] Yu[41] discussed the effect of temperature rise in front of a growing interface on the growth velocity of martensite in the preburst region and found that the temperature rise in a transformation front has an upper limit determined by the latent heat of transformation and the specific heat of the material. For an Fe-30 pct Ni alloy, ΔT_{max} is about 92 °C. In the preburst region, a growing martensite plate could be slowed down to reach a lower steady speed, because the accumulated temperature rise with the increasing size of the plate would reduce the net chemical driving force. The actual growth rate is, thus, limited by heat dissipation. When the undercooling becomes large enough, the net driving force will not be entirely offset by the maximum temperature rise ΔT_{max}, and it will keep the transformation front moving at a higher steady-state velocity. As the transformation temperature

is further lowered, the steady-state growth rate increases up to a point where it becomes large enough to create a stress wave that triggers the autocatalytic formation of neighboring martensite plates. This temperature is, thus, referred to as the "burst temperature," M_b. It seems that a few signals detected above M_b are presumably from those transformation events with relatively large growth velocity that enter the detectability range of our measuring techniques.

A large number of postburst transformation events were detected by the magnetic and acoustic emission measurements. These signals were quantitatively analyzed to derive their final size and average growth velocity. The results are shown in Figures 7 and 14. The size of martensite plates decreases with descending temperature because of the partitioning of the austenite grains. The growth velocity shows wide scattering (the velocity ratio v/v_t ranges from 0.25 to 0.65) and a slightly decreasing average value as the temperature drops. Two independent measurements in our study resulted in very consistent trends of the growth velocity.

In order to explain the velocity scatter, several possibilities should be considered. First of all, the experimental errors involved in signal measurements and analog-digital conversion are estimated to be within ± 10 pct. In the single AE transducer measurements, the takeoff angle was assumed to be 55 deg (the maximum probability direction).[34] Although we chose for further analysis only the AE signals that showed a large amplitude in the first motion, the actual takeoff angle could still to some extent deviate from the maximum probability direction. If we allow the takeoff angle to vary within ± 10 deg, the resultant error in the growth velocity is estimated to be less than ± 16 pct. Combining these two sources of error, the rms error should be less than ± 20 pct and, therefore, too small to account for the wide velocity scatter ranging from 0.25 to 0.65 v_t.

Another possible source of velocity scatter arises from variation in the actual shape of martensite plates. We have been using a circular disc model in our analysis. It is generally accepted that martensite plates in Fe-30Ni are of thin ellipsoidal shape. Although there is no thorough statistical investigation of the three-dimensional shape of martensite plates available so far, it seems plausible that the actual shape may not always be fully circular in the radial dimension. An obvious example is that some martensite plates may start growing from a grain boundary and form a semicircular disc. Thus, it is reasonable to assume that the shape of martensite plates can range statistically from semicircular to fully circular discs. This causes a variation of the estimated volume of a plate by a factor of 2. Bear in mind that the signal amplitude is proportional to the square of growth velocity. The ratio of the maximum to minimum growth velocity then can be as much as $\sqrt{2}:1$. However, this ratio is still much smaller than that observed by the quantitative measurements.

Two distinct features of the growth velocity revealed in the present study, the growth velocity scatter and the slight velocity decrease with temperature drop, can be explained in terms of varying stress and strain conditions in the vicinity of growing martensite plates. It is well established that the elastic stress and the plastic deformation may either assist or suppress martensitic transformations, depending on whether the resolved components of the acting stress on the shear planes of the transformation aid or oppose the chemical driving force. In the postburst temperature regime, a large number of martensite plates have already formed in each austenite grain. They create a complex stress and strain condition due to the dilation and plastic accommodation. The stress condition varies from one location to another. Some growth events might be assisted by the stress and strain conditions, gaining more driving force, while others might lose driving force. Therefore, it is not surprising that the growth rate of the postburst events shows a relatively wide scatter even at the same temperature. As the fraction of the transformation increases, the retained austenite regions attain more and more hydrostatic pressure, which is known to suppress martensitic transformations. This probably explains the slightly descending trend of the growth velocity with decreasing temperature in spite of the increase in the chemical driving force due to the increasing supercooling. The argument that strain conditions have a great impact on the actual growth velocity of a martensite plate is also supported by the results of the molecular dynamics computer simulations conducted by the authors in the same alloy system. These results will be described in the following paper.[42]

VII. CONCLUSIONS

1. By using a quantitative approach to the acoustic emission (AE) source characterization proposed by the authors, the growth velocity and the final size of the martensitic transformation events can be derived without getting involved in the complicated measurements of media attenuation. This method can be easily transferred to study crack growth and high rate deformation processes.
2. The magnetic induction method has been critically examined in the present study. Significant improvements have been made to eliminate various sorts of artifacts caused by the detection circuitry. Based on the relatively simple patterns of magnetic signals, we were able to characterize signal types and distinguish between single events and multievents and their corresponding temperature ranges. In order to analyze the magnetic signals quantitatively, we have studied the effect of eddy currents on the signal form and developed a method to extract information on the growth rate of each individual transformation event.
3. The magnetic and acoustic emission measurements provide independent but consistent results on the growth velocity of the martensitic transformation in an Fe-30 pct Ni alloy. We are able, for the first time, to determine the growth velocity and the final size simultaneously for individual transformation events. The experimental results indicate that the growth velocity of the athermal martensitic transformation ranges from 0.25 to 0.65 of the shear wave velocity, depending on the strain condition in the vicinity of a transformation event.

ACKNOWLEDGMENTS

We are grateful for many helpful discussions with P.E. Best, M. Cohen, J.E. Morral, and G.B. Olson. Financial support for this work was generously provided by the University of Connecticut Research Foundation and the National Science Foundation, Division of Materials Research.

REFERENCES

1. M. Suezawa and H.E. Cook: *Acta Metall.*, 1980, vol. 28, pp. 423-32.
2. P.C. Clapp: *Phys. Status Solidi B*, 1973, vol. 57, pp. 561-69.
3. T. Suzuki and M. Wuttig: *Acta Metall.*, 1975, vol. 23, pp. 1069-76.
4. G.B. Olson and M. Cohen: *Metall. Trans. A*, 1976, vol. 7A, pp. 1897-923.
5. M.S. Wechsler, D.S. Lieberman, and T.A. Read: *Trans. AIME*, 1953, vol. 197, pp. 1503-15.
6. J.S. Bowles and J.K. Mackenzie: *Acta Metall.*, 1954, vol. 2, pp. 129-47 and 224-34.
7. R. Bullough and B.A. Bilby: *Proc. Phys. Soc.*, 1956, vol. 69B, pp. 1276-86.
8. Z. Nishiyama: *Martensitic Transformation*, Academic Press, New York, NY, 1978.
9. S. Takeuchi, H. Suzuki, and T. Honda: *JIM*, Spring Meeting, 1950, p. 21.
10. R.B.G. Yeo: *Trans. ASM*, 1964, vol. 57, pp. 48-61.
11. Z.S. Basinski and J.M. Christian: *Acta Metall.*, 1954, vol. 2, pp. 148-66.
12. M. Grujicic, G.B. Olson, and W.S. Owen: *Metall. Trans. A*, 1985, vol. 16A, pp. 1713-44.
13. H.J. Wiester: *Z. Metallkd.*, 1932, vol. 24, p. 276.
14. F. Förster and E. Scheil: *Z. Metallkd.*, 1940, vol. 32, pp. 165-73.
15. R.F. Bunshah and R.F. Mehl: *Trans. AIME*, 1953, vol. 197, pp. 1251-58.
16. H. Beisswenger and E. Scheil: *Arch. Eisenhüttenwes.*, 1956, vol. 27, pp. 413-20.
17. H. Kimmich and E. Wachtel: *Arch. Eisenhüttenwes.*, 1964, vol. 35, p. 1193.
18. K. Mukherjee: *Trans. TMS-AIME*, 1968, vol. 242, pp. 1495-501.
19. T. Okamura, S. Miyahara, and T. Hirone: *Rikagaku Kenkyusho Iho*, 1942, vol. 21, p. 985.
20. Y. Suzuki and H. Saito: *JIM*, Fall Meeting, 1972, pp. 233-34.
21. L. Kaufman and M. Cohen: *Trans. AIME*, 1956, vol. 206, pp. 1393-401.
22. E.S. Machlin and M. Cohen: *Trans. AIME*, 1951, vol. 191, pp. 746-54.
23. S.S. Hsu, J.H. Chen, and P.C. Clapp: *Phys. Status Solidi A*, 1978, vol. 50, pp. 393-98.
24. R.L. Patterson and C.M. Wayman: *Acta Metall.*, 1966, vol. 14, pp. 347-69.
25. R. Datta and V. Raghavan: *Mater. Sci. Eng.*, 1982, vol. 55, pp. 239-46.
26. G.R. Speich and R.M. Fisher: *Acoustic Emission*, ASTM STP 505, 1971, pp. 140-51.
27. D.J. Goddard and J. Holt: *Acoustic Emission*, Deutsche Gesellschaft für Metallkunde, 1980, pp. 151-63.
28. H.N.G. Wadley, C.B. Scruby, and G. Shrimpton: *Acta Metall.*, 1981, vol. 29, pp. 399-414.
29. N.N. Hsu, J.A. Simmons, and S.C. Hardy: *Materials Evaluation*, 1977, vol. 35 (10), pp. 100-06.
30. C.B. Scruby and H.N.G. Wadley: *J. Phys. D: Appl. Phys.*, 1978, vol. 11, pp. 1487-94.
31. T.M. Proctor: *J. Acoustic Soc. Am.*, 1982, vol. 71, pp. 1163-68.
32. E.P. Papadakis: *J. Acoustic Soc. Am.*, 1965, vol. 37, pp. 703-10.
33. E.P. Papadakis: *J. Acoustic Soc. Am.*, 1965, vol. 37, pp. 711-17.
34. Z.-Z. Yu and P.C. Clapp: *J. Applied Phys.*, 1987, vol. 62, pp. 2212-20.
35. H. Berger: Industrial Quality Inc., Gaithersburg, MD, private correspondence, 1985.
36. G.A. Alers, J.R. Neighbours, and H. Sato: *J. Phys. Chem. Solids*, 1960, vol. 13, pp. 40-55.
37. R.S. Tebble, I.C. Skidmore, and W.D. Corner: *Proc. Phys. Soc. London*, 1950, vol. 63A, pp. 739-61.
38. R.M. Bozorth: *Ferromagnetism*, D. Van Nostrand Company, New York, NY, 1951, pp. 524-32.
39. J. Jeans: *Mathematical Theory of Electricity and Magnetism*, Cambridge University Press, 1946.
40. Z. Nishiyama, A. Tsubak, H. Suzuki, and Y. Yamada: *J. Phys. Soc. Japan*, 1958, vol. 13, pp. 1084-90.
41. Z.-Z. Yu: Ph.D. Dissertation, University of Connecticut, Storrs, CT, 1987.
42. Z.-Z. Yu and P.C. Clapp: *Metall. Trans. A*, 1989, vol. 20A, pp. 1617-29.